# Mechanism of the Electrophoretic Deposition of CdSe Nanocrystal Films: Influence of the Nanocrystal Surface and Charge

**Shengguo Jia, Sarbajit Banerjee, and Irving P. Herman***

*Materials Research Science and Engineering Center and the Department of Applied Physics and Applied Mathematics, Columbia University, New York, New York 10027*

*Received: May 1, 2007; In Final Form: September 24, 2007*

Electrophoretic deposition (EPD) leads to equally thick films of distinct colloidal CdSe nanocrystals on the positive and negative electrodes due to the deposition of equal numbers of negatively and positively charged nanocrystals, even though their concentrations are not equal in solution. EPD stops when the lower concentration charged nanocrystals, here the negatively charged nanocrystals, are depleted. These and other mechanistic features of EPD are analyzed using electrophoretic mobility (ζ-potential) analysis, photoluminescence, inductively coupled plasma−atomic emission spectroscopy, thermogravimetric analysis, and related measurements, which also show that the surface charge of nanocrystals can be substantially altered by the presence of coordinating ligands. Several cycles of nanocrystal washing are needed so the nanocrystals are able to transfer charge and/or "stick" to the electrodes upon electrophoretic deposition.

## 1. Introduction

Colloidal particles are conventionally stabilized in solution by repulsive electrostatic interactions.[1] The surface charge on nanocrystals can strongly influence their properties with implications for several proposed applications. However, only recently has the role of charge been examined for colloidal nanocrystals that are soluble in organic solvents.[2−6] The charge on nanocrystals can be used to assemble these materials into novel films and superlattice structures. For example, by carefully controlling the evaporation of the solvent, Shevchenko et al. have obtained binary superlattices composed of different kinds of colloidal nanocrystals.[7,8] Different stacking patterns were obtained by modifying the electrostatic interactions between the nanocrystals by adding different organic ligands that bind to the nanocrystal surfaces. Mandal et al. have demonstrated that peptide-functionalized gold nanoparticles can be reversibly switched between 1D and 2D patterns by tuning the pH of the nanoparticle solutions.[9] Mattoussi and co-workers have measured the electrophoretic mobility of CdSe nanocrystals capped by hydrophilic ligands and have found the mobility to vary significantly depending upon the lateral extent of the hydrophilic surface coating.[10]

In a previous report, we demonstrated an electrophoretic deposition (EPD) method for making smooth and robust CdSe nanocrystal films on conductive substrates, such as gold-coated Si or indium−tin−oxide (ITO)-coated glass.[11] The EPD of 3.2 nm CdSe nanocrystals produced several μm thick films on both electrodes with equal thicknesses, while the current through the solution decreased with time.[11] It was suggested that the equally thick films on the electrodes implied that there were equal concentrations of positively and negatively charged CdSe nanocrystals in the hexane/octane solution. Subsequently, we showed that the smoothest films were deposited when these nanocrystals were washed (reprecipitated) two or three times before EPD.[12] A washing process consists of the flocculation of the particles by the addition of methanol to the hexane/octane solution, followed by centrifugation to collect the nanocrystals and redispersion of the nanocrystals in hexane. Once-washed nanocrystals barely formed films. Nanocrystals that were washed more than three times produced rough, clumpy films. These observations were explained by the partial loss of capping ligands in each washing cycle. Obtaining a deeper understanding of the deposition mechanism requires a more detailed study of the CdSe nanocrystal surface and charge. This study details the steps involved in EPD by coupling elemental analysis and electrophoretic mobility measurements of the CdSe nanocrystals with deposition studies for a range of nanocrystal core sizes.

## 2. Experimental Methods

CdSe nanocrystals (2.3, 3.2, and 5.0 nm semiconductor core diameters) capped by *n*-trioctylphosphine oxide (TOPO) and trioctylphosphine (TOP) were synthesized by the decomposition of dimethylcadmium, as reported by Murray et al.,[13] using a molar ratio of selenium to cadmium precursors of 1.3. Studies were conducted on solutions of each of these nanocrystals and on mixtures of 2.3 and 5.0 nm nanocrystals.

After synthesis, these nanocrystals were washed for a number of cycles, with each cycle consisting of the addition of methanol to flocculate the nanocrystals from hexane/octane solution, collection of nanocrystals by centrifugation, and redissolution in 9:1 (v/v) hexane/octane. As shown in earlier work,[11] qualitatively similar results were obtained using hexane, octane, or hexane/octane mixtures as the solvent; the hexane/octane mixture was used here for consistency with most of the work reported earlier.[11,12,14] This solution was used to deposit the CdSe nanocrystal films on conductive electrodes (gold-coated silicon) with the application of a high dc voltage (500 V). The nanocrystals prepared by these washing cycles are referred to as 1×, 2×, etc., depending upon the number of cycles. During the deposition, the dc current was recorded as a function of time. The thickness of the nanocrystal films was measured by profilometry.[15]

* To whom correspondence should be addressed. E-mail: iph1@columbia.edu. Phone: 1-212-854-4950. Fax: 1-212-854-1909.

10.1021/jp0733320 CCC: $40.75 
Published on Web 12/13/2007

The electrophoretic mobility measurements of the CdSe nanocrystal solution were made before and after EPD by using a Malvern Zetasizer NanoZS instrument with irradiation from a 632.8 nm He−Ne laser. The samples were filled in dip cells fitted with Pt electrodes with a pair of electrodes separated by 2 mm. An alternating square voltage was applied during the measurement process (with a nominal voltage of 40 V and an effective voltage of 39.2 V). Each presented plot represents an average of four measurements, and each measurement consists of 200 repetitions of a 2-s long scan. All data were collected at 25 °C. The combination of laser Doppler velocimetry and phase analysis light scattering (PALS) allows the determination of the entire electrophoretic mobility distribution for a given species instead of only an average mobility. Only data with clear changes in phase with varying voltage are presented. This instrument was also used to measure nanocrystal sizes by elastic light scattering.

Although the electrophoretic deposition of the nanocrystal films was performed in a 9:1 (v/v) hexane/octane mixture, all the electrophoretic mobility and ζ potential measurements were conducted in chloroform because of systematic changes in time of the mobility curves and phase plots in hexane/octane, presumably because the nanocrystals were being electrophoretically deposited onto the electrodes of the dip-cell. "Null" run control experiments were conducted in which the nanocrystals were treated in exactly the same way as during EPD except that no voltage was applied.

Nanocrystals were transferred to chloroform in two ways. In method 1 most (but not all) of the hexane/octane was allowed to evaporate and then chloroform was added. In method 2 chloroform was added to the hexane/octane solution and then most of it was allowed to evaporate and more chloroform was added, followed by evaporation and the further addition of chloroform. The solvent was never allowed to evaporate totally because dried nanocrystals aggregate and do not dissolve well again. (Both methods gave semiquantitatively the same results, but nanocrystals transferred by method 1 sometimes tended to flocculate and this prevented the recovery of all the nanocrystals for the postdeposition measurement.) When the mobility of the nanocrystals was studied versus the number of washing cycles, chloroform was added directly to the samples after centrifugation (method 3). Good phase plots were obtained for the 2.3 and 3.2 nm nanocrystals but not always for the 5.0 nm nanocrystals because these nanocrystals were more prone to flocculation (and so mobility data are not presented for these large nanocrystals).

There could be differences in the charge distribution of nanocrystals in chloroform and that in hexane/octane because of different counterions and co-ions—in part because chloroform is slightly more polar (and there can also be differences in the mobility due to different solvent viscosities). However, the important findings do not seem to be affected by this change in solvent, as is described below.

Inductively coupled plasma−atomic emission spectroscopy (ICP−AES) (Desert Analytics, Tucson, AZ) was used to determine the Cd/Se ratio and the P/Cd and P/Se ratios, which was used to determine the number of TOPO and TOP ligands on the surface. Thermogravimetric analysis (TGA, TA instruments) was also used to compare the amounts of cores and ligands with each washing cycle, by comparing the nanocrystal mass after heating in oxygen to ∼100 °C, to remove residual solvent, and then up to ∼700 °C, to remove the ligands.

In several runs, the CdSe nanocrystal solution was monitored before and after deposition by UV−visible transmission spectroscopy (Agilent). This gave the numbers of nanocrystals in the cell before and after deposition—and therefore the numbers of nanocrystals deposited—by using the cell volume and the concentration of the CdSe nanocrystal solution, which was determined using Beer's law,[16] the absorbance of the solution, and the empirical extinction coefficients of the first exciton peak reported by Yu et al.[17] The number of deposited nanocrystals was also determined from the fractional change in absorption, TGA, and ICP-AES analysis [to determine the ratio of the core mass (from the Cd and Se atoms) and the ligand mass (from the P atoms)]. The third way the number of deposited nanocrystals was determined was from the volume of the deposited films and the packing fraction.

Room-temperature photoluminescence (PL) spectra were obtained using excitation by the 488 nm line of an Ar-ion laser (Coherent), with backscattering collection and analysis by an Ocean Optics spectrometer (Ocean Optics USB 2000).

**TABLE 1: Numbers of Atoms (from ICP-AES) and Ligand Sites [Calculated from the Number of Atoms within 0.262 nm of the Surface (Expected) and Assuming a Shell of TOPO Molecules (Maximum, Shell)] of CdSe Nanocrystals with Different Core Diameters Subjected to Different Numbers of Washing Cycles, Using a Spherical Nanocrystal Assumption**

| nanocrystal type | Cd atoms | Se atoms | core atoms | ligand sites (expected) | ligand sites (max, shell) | P atoms |
|---|---|---|---|---|---|---|
| 1× 2.3 nm | 131 | 95 | 226 | 122 | 104 | 100 |
| 4× 2.3 nm | 131 | 96 | 227 | 122 | 104 | 55 |
| 5× 2.3 nm | 131 | 95 | 226 | 122 | 104 | 50 |
| 1× 3.2 nm | 342 | 274 | 616 | 256 | 155 | 454 |
| 2× 3.2 nm | 341 | 275 | 616 | 256 | 155 | 205 |
| 3× 3.2 nm | 340 | 277 | 617 | 256 | 155 | 191 |
| 1× 5.0 nm | 1236 | 1142 | 2378 | 672 | 288 | 841 |
| 2× 5.0 nm | 1270 | 1093 | 2363 | 668 | 288 | 481 |
| 4× 5.0 nm | 1272 | 1091 | 2363 | 668 | 288 | 278 |

## 3. Results

The core diameters of the nanocrystals synthesized (2.3, 3.2, and 5.0 nm) were determined using the peaks of the first-exciton absorption features (510, 546, and 609 nm) and the calibration in ref 17.

**3.1. Atomic Composition of CdSe Nanocrystals.** The relative atomic compositions of Cd, Se, and P of the nanocrystals were determined by ICP−AES. These data are presented in Table 1 as the numbers of atoms/nanocrystal (listed as "core atoms") by using the given total number of atoms in the core from ref 18 for the respective core radii (and assuming that the cores are spheres). (See also Table S1, and Figure S1 and Table S2 for TGA analysis in the Supporting Information.)

**3.2. Electrophoretic Mobility Measurements.** The measured electrophoretic mobilities, $\mu_e$, are also presented in terms of the ζ potential by using the Henry equation, $\mu_e = 2\epsilon\zeta f(\kappa r)/3\eta$, where $\epsilon$ is the dielectric constant of the solvent, $\eta$ is the viscosity of the solvent, and $f(\kappa r)$ is Henry's function with Debye screening parameter $\kappa$ (and Debye length $1/\kappa$) and particle geometric radius $r$.[10,19] Using the Huckel approximation for small particles in low dielectric constant media, $f(\kappa r) = 1$, and $\epsilon = 4.8$ and $\eta = 0.542$ cp for chloroform, a 10 mV ζ potential corresponds to a mobility of 0.05227 (μm cm)/(V s), and this conversion is used here.

Figure 1a shows the ζ potential distributions of solutions of 1×, 2×, and 3× 3.2 nm nanocrystals prepared in chloroform by method 3. For the ζ potential measurements, we determine the fraction of the area of the profile for which the ζ potential is negative (herein called the "negative" fraction, $f_n$); the fraction

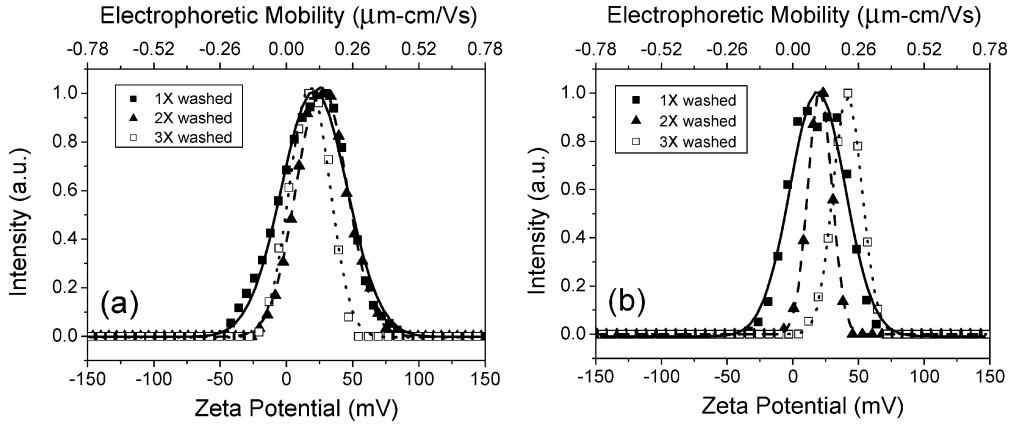


**Figure 1.** ζ potential and mobility distributions of (a) 3.2 nm and (b) 2.3 nm CdSe nanocrystal solutions as a function of the number of washing cycles (transferred from hexane/octane to chloroform using method 3). (See Table S3.)

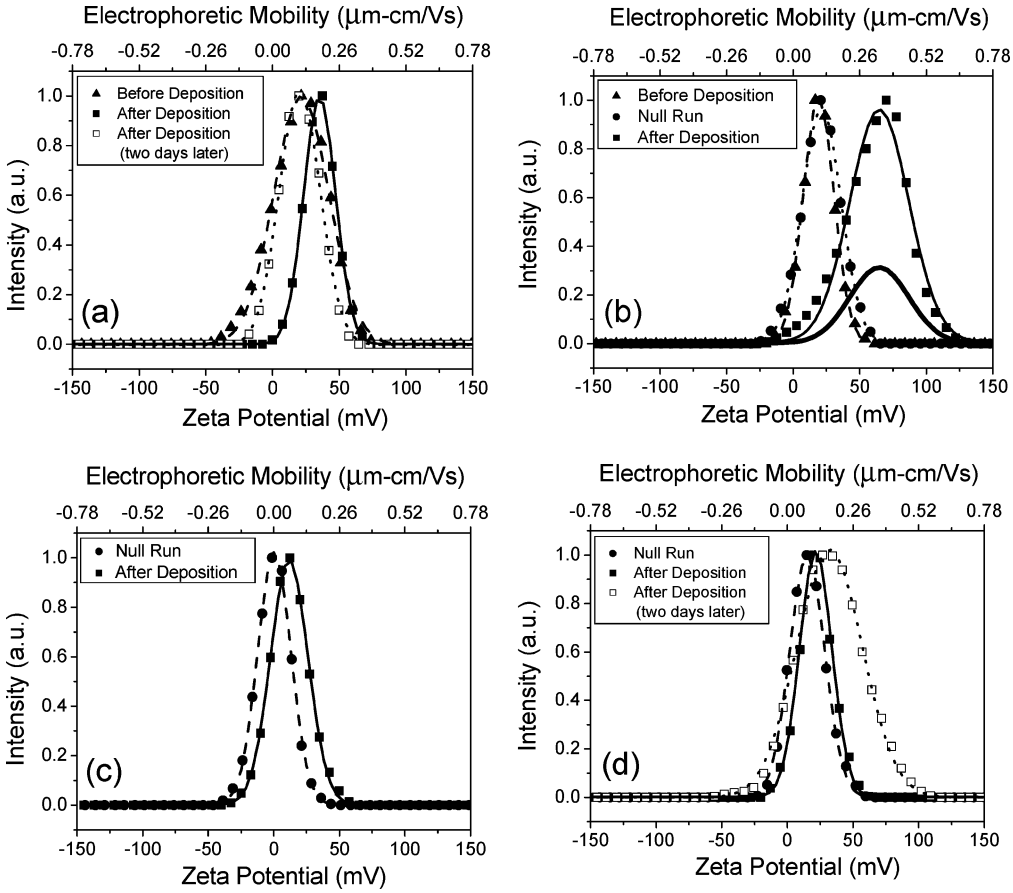


**Figure 2.** ζ potential and mobility distributions of (a) 2× 3.2 nm (Table S4, run 1), (b) 2× 3.2 nm (Table S4, run 4), (c) 4× 2.3 nm (Table S5), (d) 5× 2.3 nm (Table S5) CdSe nanocrystal solutions before deposition (a, b), after deposition, and after a "null" run (b−d). Parts a and d also show results 2 days after deposition. Method 1 was used for transfer in (a), and method 2 in (b)−(d). The thick line in part b also shows the distribution after deposition with the integrated area normalized to that before deposition times the fraction of nanocrystals remaining after deposition (from Figure 3).

of the area for which the potential is positive ("positive" fraction, $f_p$) is clearly $f_p = 1 - f_n$. (These fractions would represent the fractions of the complex particles (nanocrystals plus counterions plus coions) that are respectively negatively and positively charged, only if there were no neutral nanocrystals and if the instrumental measurement line width were very small.) For these nanocrystals the negative fraction is ∼8−20%. The peak potential and width (fwhm) of these distributions are given in Table S3 (in the Supporting Information), along with the negative fraction. There is no systemic change in the distribution for successive washings of 3.2 nm nanocrystals. Figure 1b and Table S3 give the ζ potential distributions for 2.3 nm nanocrystals, for which there is a systematic trend to a smaller negative fraction with further washing, from ∼18.1% (1×) to ∼0.3% (3×).

Figure 2a,b shows the ζ potential distribution of 2× 3.2 nm nanocrystals before and after EPD for two runs. (These are runs 1 and 4 of the four runs described in Table S4 in the Supporting Information.) Figure 2a shows run 1, with the nanocrystals transferred to chloroform using method 1. Before deposition, the ζ potential of the nanocrystal solution is asymmetric, with an average value of 20.6 mV, peak width (fwhm) of 44.9 mV, and a negative fraction of 18.0% (Table S4, run 1). After EPD proceeded to form films of the maximum thickness possible

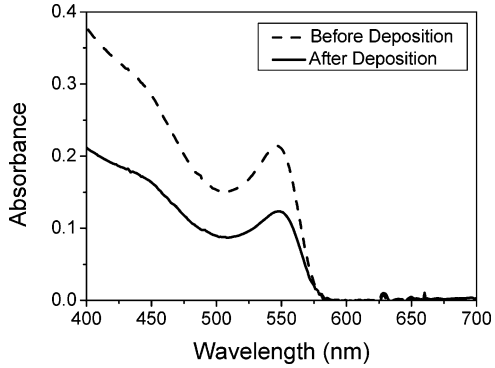


**Figure 3.** Transmission spectra of the 2× 3.2 nm CdSe nanocrystal solution before and after deposition (plotted in terms of the absorbance, assuming no scattering loss). (See Figure 2b and Table S4, run 4.)

(1100 nm in this case), there was a dramatic change, with the peak shifting toward the positive and the profile becoming much narrower, and the negative fraction was then only 0.4%. This general trend that the negative fraction decreases to nearly zero with the formation of the thickest possible films was also seen in the other three runs with 3.2 nm nanocrystals in Table S4, decreasing from 36.3% to 1.3%, 21.5% to 4.3%, and 5.8% to 1.9%, respectively for runs 2−4, although other details of the shape of the ζ potential curve were sometimes different. (Sometimes they were much broader or had multiple peaks.) In several runs, the transmission of the nanocrystal solution was measured before and after deposition (as in Figure 3 for run 4), showing that the fraction of nanocrystals deposited was 79.0%, 51.4%, and 40.9% respectively for runs 2−4 (Table S4). In Figure 2b the ζ potential distribution after deposition is also plotted with its area normalized to the area of the distribution before deposition times the fraction of nanocrystals remaining in solution (as measured by transmission). This emphasizes the change in the distribution for positive ζ potential as a result of EPD. (This change is larger in this run than in many others.) Light scattering experiments (Figure S2 in the Supporting Information) suggest that aggregate formation is usually not important during EPD.

The solution in the run shown in Figure 2a (Table S4, run 1) that had been transferred to chloroform right after EPD of the thickest films possible was remeasured after 2 days; the ζ potential distribution shifted to lower potentials, and the negative fraction had increased to 8.8%. Part of the solution remaining after deposition was used in an EPD run with new electrodes 2 days later and showed more deposition—the formation of ∼100 nm thick films. Most of the deposition occurs within the first 10 min, with no further increase in thickness noted after 30 min.

Figure 2b (Table S4, run 4) shows the results of another EPD experiment using 2× 3.2 nm nanocrystals, this time with transfer to chloroform by method 2; the results are similar to those in Figure 2a, with the negative fraction again decreasing to almost zero when the films were grown to a maximum thickness, which was 750 nm here. This figure also shows the results of a control "null" experiment in which all the procedures of the deposition run were followed except no voltage was applied across the electrodes. There is no deposition on the electrodes, and the ζ potential profile was virtually the same as that of the initial stock solution, so no significant changes were induced by the electrodes.

Clearly, there is some variability in the results using 3.2 nm nanocrystals from different synthesis runs (Figure 2a,b, Table S4); however, there was consistency in all major trends and

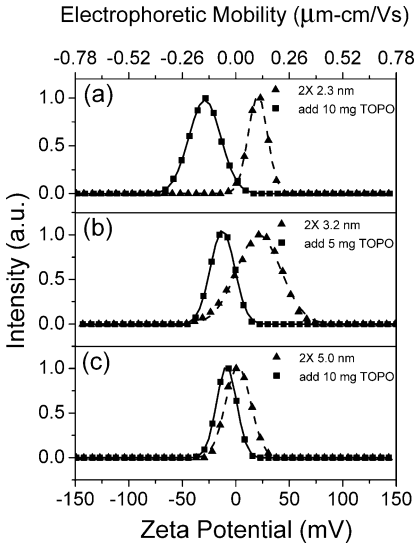


**Figure 4.** ζ potential and mobility distributions of (a) 2× 2.3 nm, (b) 2× 3.2 nm, and (c) 2× 5.0 nm CdSe nanocrystal solutions before and after the addition of TOPO to 1 mL of the solution (method 3). (See Table S6.)

most notably that when EPD terminates, the negative fraction, and consequently presumably the concentration of negatively charged nanocrystals, has decreased to nearly zero.

The smaller 2.3 nm nanocrystals show analogous behavior, as shown in Figure 2c,d and Table S5 (in the Supporting Information). The nanocrystals were transferred to chloroform by method 2. Here, during extended EPD the negative fraction decreases to nearly zero for the 5× nanocrystals (from 13.7% to 4.7%) but not for the 4× nanocrystals (from 48.8% to 18.7%). In these two runs, 20.0% and 15.6% of the nanocrystals were deposited, respectively, as determined by transmission (Figure S3 in the Supporting Information).

Figure 4 (Table S6 in the Supporting Information) shows that adding TOPO (to the solution after transfer to chloroform) respectively to the 2× 2.3, 3.2, and 5.0 nm nanocrystals decreases the ζ potential to more negative values, from 20.1 to −28.1, 20.6 to −10.4, and 3.8 to −8.3 mV, and increases the negative fraction, from 1.9% to 97.4%, 18.0% to 86.8%, and 38.6% to 81.0%. This change is most pronounced for the 2.3 nm nanocrystals. Such changes are also seen for the 2× 3.2 nm CdSe nanocrystal solution after EPD.

For mixtures of 4× 2.3 nm and 2× 5.0 nm nanocrystals, the negative fraction was 19.9% before deposition and 0.2% after deposition terminated (and 22.1% after a "null" run) (method 2 transfer), and so the negative area also seems to be depleted after EPD is completed. (See Figure S4 and Table S7 in the Supporting Information.) Using transmission to track concentrations, 70% of the 2.3 nm nanocrystals (initial concentration of $3.32 \times 10^{15}$ dots/cm$^3$) and 86% of the 5.0 nm nanocrystals ($1.89 \times 10^{14}$ dots/cm$^3$) were deposited during this EPD run. (In another run, 47% of the 2.3 nm and 51% of the 5.0 nm nanocrystals were deposited.) This shows that roughly the same fraction of each nanocrystal is deposited during these runs, and this occurs on both electrodes.

**3.3. Film Deposition and Morphology.** Using the 2.3 nm nanocrystals, no EPD films were formed using the 1× or 2× nanocrystals; thin, patchy, or no films were deposited using the 3× nanocrystals; thick, smooth films of equal thickness were deposited on both electrodes using the 4× or 5× nanocrystals. Using the 3.2 nm nanocrystals, very thin or no films were deposited using the 1× nanocrystals. Thick, smooth films of

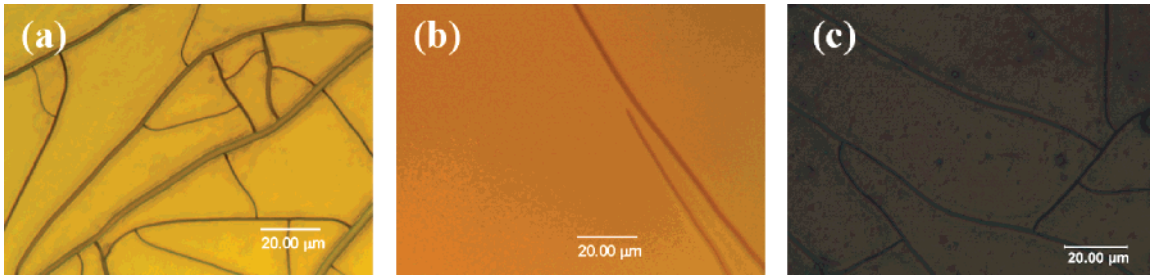


**Figure 5.** Optical micrographs of nanocrystal films prepared by the electrophoretic deposition of CdSe nanocrystals to a thickness above the threshold thickness for crack formation in each case. (The scale bars represent 20 $\mu$m.) (a) 1000 nm thick film from 4× 2.3 nm nanocrystals; (b) 1200 nm film from 2× 3.2 nm nanocrystals; (c) 2000 nm thick film from 2× 5.0 nm nanocrystals.

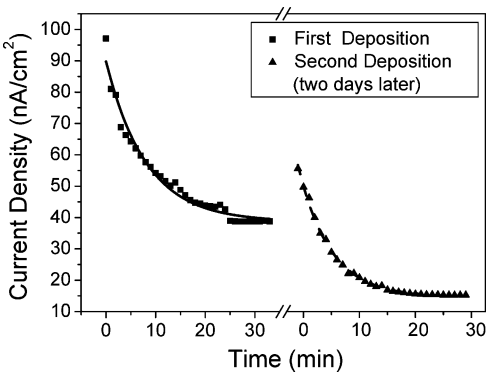


**Figure 6.** Current density vs time measured during the electrophoretic deposition of 2× 3.2 nm CdSe nanocrystals, with the deposition and measurement repeated 2 days later using the exact same solution.

equal thickness were deposited on both electrodes using the 2× nanocrystals, and thick but somewhat patchy films were deposited using the 3× nanocrystals. Using the 5.0 nm nanocrystals, very thin or no films were deposited using the 1× nanocrystals. Thick, smooth films of equal thickness were deposited on both electrodes using the 2× nanocrystals, and thick but very patchy films were deposited using the 3× nanocrystals. When thick films were deposited, the films on both electrodes were the same thickness. Films did not form when chloroform or chloroform/hexane (25%/75% v/v) mixtures were instead used as the solvent; all films described herein were deposited with hexane/octane as the solvent.

Figure 5 shows optical images of the thick deposited films for each size nanocrystals—each washed the number of times needed to obtain the smoothest films. Dried EPD films fracture, after removal from the solvent, above a threshold thickness (~800 nm for 3.2 nm nanocrystals) due to the evaporation of the residual solvent,[11] and each of these films is above the threshold thickness. The colors in the film, yellow, orange-red, and black, are consistent with the differing absorption profiles of the nanocrystals, with first exciton peaks at 510, 546, and 609 nm, respectively.

In most runs, films were deposited until they reached a final maximum thickness, usually ~0.2−3 $\mu$m (in ~45 min). The dc current across the electrodes decreased to a minimum and remained at that current afterward (Figure 6).[12,14] Roughly half of the nanocrystals then remained in solution, as monitored by transmission spectroscopy (Figure 3); the exact fraction varied with the details of the run (and likely to run-to-run variations in the capping ligands).

EPD using mixtures of 4× 2.3 nm and 2× 5.0 nm nanocrystals produced films of equal thickness on both electrodes, which were a bit rougher than those deposited from one size of nanocrystal.

When TOPO was added directly to the 2× 3.2 nm nanocrystal solution used for EPD, no deposits were formed (even though the current increased). When TOPO was added to the solution after EPD, as in Figure 4, the films on the electrodes dissolved.

**3.4. Current Collected and Nanocrystals Deposited during Deposition.** Figure 6 shows the change in the current density as a function of time during the EPD of 2× 3.2 nm nanocrystals (500 V). After 35 min, the current density dropped from 97 to 39 nA/cm$^2$, and the nanocrystal films on both the positive and negative electrodes grew to the same final thickness, ~1100 nm. After EPD, part of the nanocrystal solution was transferred to chloroform (by method 1) for mobility measurements and part remained in hexane/octane for 2 days, from which new thin films (~100 nm thick) were deposited on fresh Au electrodes. The concentration of the remaining nanocrystals was too low for reliable electrophoretic mobility measurements.

The charge collected during a 45 min long EPD run of 3.2 nm nanocrystals was ~$1.2 \times 10^{15}$ elementary charges (after subtracting the background current). Using this, the ratio of the number of nanocrystals deposited to the number of charges collected was ~10.3 (using absorbance and the absorption cross section), ~3.3 (using absorption changes, TGA, and ICP-AES),[17] and ~2.2 [using the film volumes and a random loose packing fraction of 0.58 and hard sphere core diameter of 4.6 nm (3.2 nm core diameter plus twice the 0.7 nm nominal shell thickness of TOPO[10]) and ~2.8 and ~2.4 for hcp close packing fraction of 0.74 and random close packing fraction of 0.64[20−22]].

The addition of TOPO after EPD had terminated led to a short-lived spike in the current that was not accompanied by any further discernible increase in thickness of the nanocrystal films.

**3.5. Photoluminescence of CdSe Nanocrystal Films and Solutions.** Figure 7 shows that the PL spectra of films deposited from 4× 2.3 nm nanocrystals are characterized by a very strong, broad emission peak between 660 and 720 nm, red-shifted from the exciton peak near 515 nm. The PL spectrum of films deposited from 2× 3.2 nm nanocrystals have a weak broad emission peak between 660 and 720 nm, red-shifted from the exciton peak near 570 nm. The exciton peak is near 630 nm in the PL spectra of the 2× 5.0 nm nanocrystal films, and the broad red-shifted peak is not seen. For each type of nanocrystal, the PL spectra of the as-prepared nanocrystal solutions and those used for deposition (after several washing cycles) are similar to those of the respective EPD films.

## 4. Discussion

The electrophoretic deposition of nanocrystals involves a series of steps: (1) The colloidal nanocrystals develop a charge, either during synthesis and/or as a result of processes in solution after synthesis, that depends on the ligands and solvent. (2) Charged species, including these nanocrystals, possible ag-

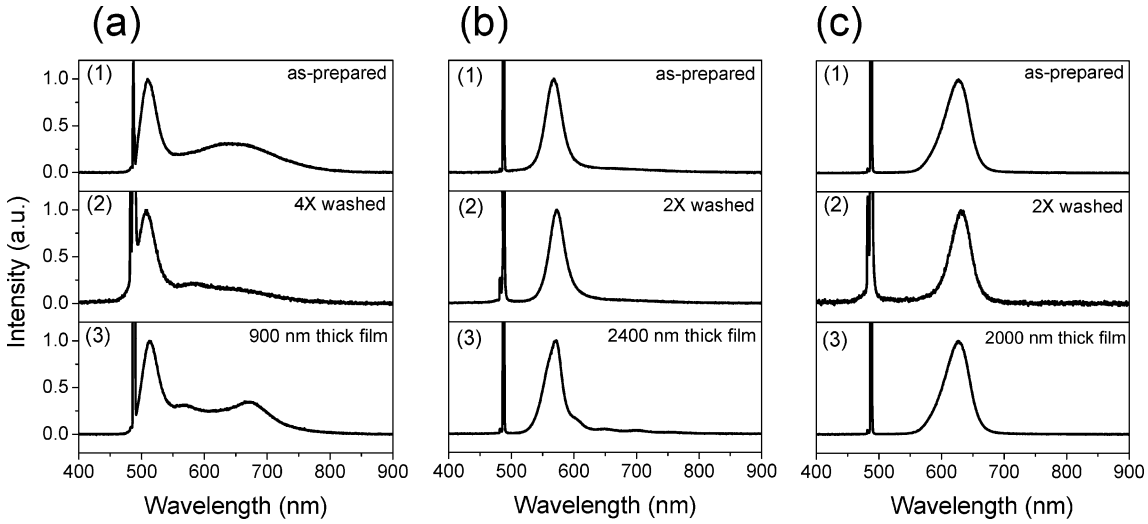


**Figure 7.** Photoluminescence of CdSe nanocrystal solutions (1) as prepared in the original solution (TOPO, butanol, and hexane) and (2) washed in hexane/octane (90%/10% v/v) and of (3) EPD films prepared from these washed nanocrystals, excited by 488 nm, for (a) 2.3 nm (4×, 900 nm thick film), (b) 3.2 nm (2×, 2400 nm thick film), and (c) 5.0 nm (2×, 2000 nm thick film) CdSe nanocrystals.

gregates of these nanocrystals, and any counterions and co-ions surrounding them are transported to the electrode surfaces under the influence of the dc electric field. (3) Charge is transferred from the nanocrystals and possibly other charged species to the electrode surface, and then it is transported through the film and to the electrode. (4) The neutral nanocrystals stick onto the surface of the existing film. Each of these steps is now discussed further.

**4.1. Nanocrystals in Solution.** *4.1.1. Ligands and Atomic Composition of CdSe Nanocrystals.* The ICP−AES measurements (Tables 1 and S1) show that the Cd to Se ratio does not change (within experimental error) with the number of washing cycles. It is unlikely that there are soluble Cd or Se complexes in solution that are trapped with the nanocrystals before analysis because any such impurities would likely be preferentially lost with each washing step. The Cd to Se ratio is larger than one and decreases with nanocrystal size, which suggests there are more Cd atoms on the surface than Se atoms.

The total number of Cd and Se surface atoms is first estimated by assuming that the nanocrystals are spherical and that atoms residing within a shell equal to the CdSe bond length of 0.262 nm[18] can be considered surface atoms, and this number is presented as "ligand sites (expected)" in Table 1. This procedure suggests the Cd atoms occupy 63−64% of the surface sites on the 2.3, 3.2, and 5.0 nm nanocrystals. This calculation is consistent with the estimate by Majetich et al.[23]

The surface of the CdSe core is passivated by TOP and TOPO ligands. Cd atoms at the surface are thought to be coordinated by TOPO molecules, whereas the Se atoms at the surface are bound to TOP (to give TOPSe).[24] Since each ligand, TOPO (bound to Cd) or TOPSe, has only one P atom, the number of P atoms/nanocrystal represents the number of ligands/nanocrystal and the ratio of the number of P atoms to the number of actual surface sites shows the extent to which the surfaces are passivated. In Table 1, the number of P atoms (or ligands) is smaller than the number of expected surface atoms for each nanocrystal except for the 1× 3.2 and 5.0 nm nanocrystals. Since at most one ligand can bind per surface site, this could indicate an underestimate of the number of available surface sites, the presence of ligands trapped by the core-bound ligands (and that are not directly bound to the core), or ligands in solution that remain with the nanocrystals after drying. It is difficult to differentiate between the last two possibilities by most analytical methods because of the similar chemical environments of excess ligands trapped by core-bound ligands and ligands present in solution; however, the below discussion of the TGA results suggests there may be some free TOPO in 1× 3.2 nm nanocrystals.

For each nanocrystal, the number of P atoms, and consequently ligands, per nanocrystal decreases with the number of times it was washed. This is consistent with our previous observations[12] for EPD films formed using 3.6 nm CdSe nanocrystals that infrared absorption by the ligands decreased with more nanocrystal washing cycles. Except for the 1× 3.2 and 5.0 nm nanocrystals, not all of the "expected" surface sites have ligands.

Because of steric factors, it may not be possible for all of the estimated surface atoms to bind ligands. The maximum number of ligands that can reside in a monolayer around a nanocrystal is estimated by assuming there is a shell of ligands about the spherical core (with no voids), with a thickness equal to the maximum possible length of a single TOPO molecule (1.6 nm—using the bond lengths of C−C, C−H, Cd−P, and P═O bonds as 1.54, 1.1, 3.0, and 1.5 Å, respectively, and the bond angle for C−C bonds as 109.47° [25]—and this is larger than the 0.7 nm shell thickness[10] used elsewhere for the hydrodynamic radius and the packing fraction). For 3.2 nm nanocrystals, this ligand-shell volume is 116 $nm^3$. Using a bulk density of TOPO of ∼0.8−0.9 $g/cm^3$ (as is typical of organic molecules), the volume of a single TOPO molecule is ∼0.71−0.80 $nm^3$ and the maximum number of TOPO ligands that can be accommodated in the ligand shell is ∼155. Table 1 gives this estimate for each nanocrystal (ligands; max, shell). In each case it is smaller than the number of estimated surface sites (expected ligand sites), and this suggests that passivation of all the surface sites by TOPO (or TOPSe) molecules is not possible due to steric reasons (within the limits of these rather crude estimates).[26] This estimate is very roughly consistent with the number of P atoms measured for the multiply washed 3.2 and 5.0 nm nanocrystals.

The numbers of atoms/nanocrystal in Table 1, assuming spherical cores, is likely an underestimate due to the presence of facets and edges on the nanocrystals. However, the major conclusions reached above are essentially the same if another extreme condition is assumed, that the nanocrystals are cubes with core length equal to the sphere diameters in Table 1, with

results shown in Table S1. For example, the fraction of core surface sites occupied by Cd is largely the same, 63−65%.

The TGA analysis of 1× to 4× washed 3.2 nm CdSe nanocrystals under $O_2$ (Figure S1 and Table S2) shows that the weight loss attributed to ligands decreases with more nanocrystal washing cycles, suggesting there are fewer ligands with more washing (282, 85, 82, and 79 respectively per core for 1×, 2×, 3×, and 4×). The trends are the same as are seen with ICP−AES, but roughly half as many ligands are measured by TGA as are by ICP−AES. Quantitative analysis by TGA may be less reliable because of the dependence on the ramping rates and the uncertain character of the decomposition products (Cd and Se oxidations, remaining product from ligand oxidation, and so on). Still of note, the number of ligands lost in TGA from ∼100 to 230 °C is significant and large only for 1× washed nanocrystals and seems to be free TOPO, because pure TOPO has a similar TGA trace. (This number of ligands roughly equals the difference in ligand numbers in 1× and 2× washed nanocrystals determined by ICP−AES.) Ligands lost from ∼230 to 400 °C, called here loosely bound ligands, and those lost from ∼400 to 700 °C, strongly bound ligands, are roughly constant with continued washing and sum to ∼80 for 2× to 4× washed nanocrystals.

The broad deep trap emission between 660 and 720 nm in the photoluminescence spectrum (Figure 7) has been ascribed to TOPSe species on the nanocrystal surfaces.[24] The TOPSe species remain strongly bound to the nanocrystals and are not easily removed during washing (in contrast to the TOPO ligands bound to Cd). Thus washing reduces the intensity of the band-edge peak (by removing passivating ligands from the surfaces), while the deep-trap peak remains unaffected. Notably, the emission from the deep trap states is much more intense for the 2.3 nm nanocrystals (Figure 7a) than the 5.0 nm nanocrystals (Figure 7c), due to the relatively larger surface-to-core ratio in the smaller nanocrystals. This corroborates the assignment of these broad peaks to surface states or, more specifically, to TOPSe species on the nanocrystal surfaces.

This suggests that TOPO molecules loosely bound to the nanocrystal surfaces are removed during washing. Surface charges are induced at the sites from which TOPO and TOPSe have been removed; however, how the loss of these ligands improves charge transfer at the film or nanocrystal adsorption after this charge transfer may be even more significant.

*4.1.2. Nanocrystal Charge.* Murray and co-workers have proposed that methanol replaces TOPO at some of the surface sites after the washing process.[24] Indeed, replacement of surface ligands with solvent molecules and surface reconstruction or oxidation phenomena likely play an important role in determining the overall charge of the nanocrystals. Krauss and co-workers have detected surface charging in CdSe nanorods by electrostatic force microscopy, which they attribute to the summation of uncompensated internal electric polarizations.[27] Similarly, exposed polar unit cells in the nanocrystal lattice may lead to the charging in nanocrystals, especially upon the removal of the passivating TOPO and TOPSe species.

The electrophoretic mobility, $\mu_e$, is $\mu_e = Ze/3\pi\eta a$, where $\eta$ is the viscosity of the solvent, $Z$ is the electrical charge in units of elementary charge $e$, and $a$ is the hydrodynamic diameter of the particle. The particle charge as analyzed here, $Ze$, is that of the nanocrystal core and ligands, as partially countered by the counterions that travel with the particle as it moves under the influence of the electric field. For singly charged nanocrystals in chloroform ($\eta = 0.542$ cP [28]), the mobilities and $\zeta$ potentials are 0.85 ($\mu$m cm)/(V s) and $\zeta = 162$ mV for a 2.3 nm core diameter (1.85 nm radius), 0.68 ($\mu$m cm)/(V s) and $\zeta = 130$ mV for a 3.2 nm core diameter (2.3 nm radius), and 0.49 ($\mu$m cm)/(V s) and $\zeta = 94$ mV for 5.0 nm core diameter (3.2 nm radius). (This uses an estimate of the TOPO shell thickness of 0.7 nm.[10]) The measured values are smaller than these estimates because of partial screening of the core charge and the increase in the hydrodynamic radius by counterions. Any aggregation would also decrease them.

These reasons and broadening explain why quantitative analysis of the charge distribution is difficult, including discounting the possibility of multiply charged nanocrystals, even though profiles with distinct multiple peaks in the profiles are seldom seen. Consequently, relative positive and negative areas in the $\zeta$ potential/mobility plots do not necessarily give the relative concentrations of positive and negative ions, even if all ions were singly charged and if there were no neutral nanocrystals.

Nevertheless, it is clear that when EPD films grow to equal thicknesses on both electrodes and then EPD stops and the current becomes constant, the negative fractions (usually) approach zero, and this suggests that there are (1) initially more positively charged ions than negatively charged ions, (2) counterions are present in solution to maintain charge neutrality (even with the nonpolar hexane/octane solvents, and there are at least negative counterions) in these cases, (3) an equal number of positively and negatively charged nanocrystals are deposited (and transfer their charge), (4) none of the nanocrystals were neutral before deposition (unless they became charged during deposition), (5) EPD terminates because the negative nanocrystals are absent, and (6) the primary contribution to the current is from charge transfer from charged nanocrystals at the electrodes (and counterions are not substantially involved because the film thicknesses do not reflect the relative proportions of positively and negatively charged nanocrystals).

Previously, we concluded that the equal thickness of the films means that there were equal densities of positively and negatively charged nanocrystals in solution.[11] We now believe that equal numbers of positively and negatively charged nanocrystals are removed from the solution during EPD.

It is reasonable that EPD stops when there is depletion of the minority charged nanocrystals in general, here the negative nanocrystals. However, there is no film deposition observed in cases where the negative fractions exceeds the positive fraction here (Figure 4), possibly because in this particular system there are too many ligands to permit charge transfer or sticking.

The consistency of the depletion of negatively charged nanocrystals during EPD in which the thickest possible films are grown also suggests that transferring the solution from hexane/octane to chloroform does not qualitatively change the overall conclusions. Furthermore, even though the initial negative fraction varied between runs (not unexpectantly, due to run-to-run variations in the synthesis and washing), in each case EPD continues until the negative charge appears to be depleted, and so the same conclusions can be drawn even given the experimental variability. The identification of the negative and positive area fractions with the fractions of negatively and positively charged nanocrystals is consistent with what is seen but clearly has an error associated with it, for the reasons given earlier.

There are clearly changes in the mobility profile as a result of deposition distinct from a simple depletion of part of the profile, which could be due to aggregation or changes in the charges of the nanocrystals, as is clear from the concentration

normalized mobility plots in Figure 2b. It is more likely that the depletion in the mobility profile for negative $\zeta$ potential during deposition is due to the depletion of negative nanocrystals by deposition and unlikely, as we will see, that it is due to negative nanocrystals being converted to positive ones during EPD. Even after normalization to account for the loss of nanocrystals in solution, there is a real shift to more positive voltages (and mobilities) in the distribution at positive $\zeta$ potentials as a result of EPD that could indicate an increase in nanocrystal charge (due to larger core charges or less shielding by counterions) and/or smaller nanocrystals (possibly due to decreased aggregation—however, see Figure S2). This change is more prominent in the run of Figure 2b than those for Figure 2a,c.

After all the 3.2 nm negatively charged nanocrystals have been removed from solution, deposition of positively charged nanocrystals does not proceed on the negative electrode, even with negative counterions in solution. This suggests that counterions do not transfer charge at the electrode surfaces. This also seems to be true for the EPD of 2.3 nm nanocrystals.

The initial larger number of positively charged nanocrystals (Table S4) can be rationalized by the preferential removal of TOPO in washing, which exposes Cd sites at the surface. The origin of the negatively charged nanocrystals is not clear, but there may perhaps be some nanocrystals with Se-rich surfaces.[27] Another possibility for forming negatively charged nanocrystals is the migration of TOP molecules from Se to Cd atoms on the nanocrystal surfaces (accompanied by oxidation to TOPO) or surface reconstruction upon the loss of passivating ligand molecules. The exposed Se atoms on the surface would lead to the nanocrystals becoming negatively charged. The addition of TOPO shifts mobility plots to more negative values. This suggests that the TOPO is passivating Cd surface sites that had been positive. As further corroboration of this model, Murray et al. have found that the addition of excess TOPO to a solution of CdSe nanocrystals increases the PL efficiency by around 34%,[24] which points to the passivation of surface Cd atoms by TOPO (accompanied by a decrease in nonradiative combination).

Allowing the solution transferred to chloroform to stand for 2 days after deposition seems to increase the negative fraction and allow for continued EPD. This apparent change in the charge distribution likely originates from the loss of loosely bound ligand molecules[24] or the movement of ligands on the surfaces of the remaining nanocrystals.

This discussion has focused on the 3.2 nm nanocrystals. For 4× 2.3 nm nanocrystals (Figure 2c), all the negative nanocrystals are not depleted after EPD is complete [although the fraction of negatively charged nanocrystals is significantly decreased from 48.8 to 18.7% (Table S5)], which suggests that in this case excess ligands on the nanocrystals may prevent some negative nanocrystals from sticking to the electrodes. However, when 5× nanocrystals are used, all the negative nanocrystals are depleted during deposition (Figure 2d). After 2 days, the negative area increases to 11.6% for these nanocrystals (Figure 2d, Table S5).

**4.2. Electrophoretic Deposition.** *4.2.1. Film Deposition and Properties.* The above text and Tables S4, S5, and S7 give the fraction of particles deposited during EPD as determined from transmission before and after deposition. There is run-to-run variability in this fraction that likely arises from variability in the synthesis and washing runs. These tables also give this fraction estimated from the $\zeta$ potential distributions, $2(f_{nb} - f_{na})/(1 - 2f_{na})$, where $f_{nb}$ and $f_{na}$ are the negative fractions before and after deposition. This estimate assumes that the negative fraction equals the fraction of negatively charged nanocrystals (which should not be exactly true, because of profile broadening), there are no neutral nanocrystals, and during EPD an equal number of negatively and positively charged nanocrystals deposit. This estimate is close to the fraction from transmission in most cases, which is evidence that these assumptions may be reasonable. However, there is a large difference in two runs: in Figures 2b and 3 (run 4 in Table S4, 2× 3.2 nm nanocrystals), which may be linked to the large change in the distribution at positive $\zeta$ potential associated with EPD or to the possible charge transfer at the electrodes with no concomitant nanocrystal sticking in this run, and in Figures 2c and S3a (Table S5, 4× 2.3 nm nanocrystals), which may also be linked to the possible charge transfer at the electrodes with no concomitant nanocrystal sticking or to the incomplete depletion in the negative area after EPD terminates in this run.

Clearly, some of the capping ligands need to be removed to deposit smooth films. This helps charge transfer at the electrode and/or the sticking of the neutral nanocrystal. (It may or may not strongly affect nanocrystal charge, as in Figure 1b,a, respectively.) Ligand loss during washing has been confirmed by Murray and co-workers,[24] who postulated two different kinds of TOPO ligands on the nanocrystal surfaces: loosely bound ligands (thought to be bound to vertex and edge sites) and more tightly bound ligands that are much harder to exchange or remove. Rougher films are formed using 3× and 4× nanocrystals[12] because of aggregation in solution due to the loss of some ligands (as observed by scattering at visible wavelengths which makes the solutions appear cloudy). However, even for smooth films formed from 2× 3.2 nm nanocrystals, the role of aggregates cannot be discounted. This is one possible reason why there appear to be more particles collected than elementary charges during EPD (see below); however, light scattering experiments (Figure S2) suggest that aggregate formation is usually not important. (The loss of some charged nanocrystals during the washing process cannot be entirely discounted, although such losses are likely to be minimal as suggested by the optical absorption spectra of the nanocrystals before and after washing.)

Notably, no film can be deposited using the 2× 3.2 nm nanocrystal solution with added TOPO, just as for 1× 3.2 nm nanocrystals. Although additional or excess TOPO changes the mobility profile, in most cases there still appear to be negatively and positively charged nanocrystals. Likely, the full (or excess) TOPO/TOPSe inhibits charges transfer to the surface and/or inhibits sticking of the neutral nanocrystals.

To deposit smooth and thick films from the smaller 2.3 nm nanocrystals, as many as four or five washing cycles are necessary. This observation may be related to the relatively higher ligand-to-core ratio in these smaller nanocrystals (smaller nanocrystals have a larger surface-to-volume ratio).[29]

Figure 5 shows optical images of the deposited films, indicating that the films start to fracture above a threshold thickness due to the evaporation of the residual solvent.[18] This will be addressed more elsewhere.

The PL spectrum is substantially the same for the EPD films as for the nanocrystal solutions, which suggests that EPD does not does affect the trap states; the small differences could be due to radiative transfer between nanocrystals[30] (Forster transfer).

*4.2.2. Current Flow during Deposition and Charge Transfer at the Surface.* The ratio of the electric potential across two 1 $\mu$m thick nanocrystal films and the 2 mm thick nanocrystal solution is ~1/2500, so most of the potential drop remains across

the solution and the decrease in current during EPD is not due to a change in the internal resistance of the system. (This uses the dielectric constants of CdSe, TOPO, hexane, and octane of 10.2, 2.6, 1.9, and 1.96, respectively. The concentration of the CdSe nanocrystals is $\sim 10^{15}$ nanocrystals/cm$^3$, which is less than $10^{-5}$ M, so we can use the dielectric constant of the solvent as that of the solution.)

As the films grow, the current decreases, and growth occurs to a certain thickness and the current decreases to a constant value; this termination of growth seems to occur when the negatively charged nanocrystals are depleted.

The observed current measured across the system results from charge transfer at the electrodes. Charge transfer must accompany the deposition of the nanocrystals on the electrodes since $\sim 3 \times 10^{-4}$ monolayers of singly charged nanocrystals would completely screen the applied electric field. This charge could transfer to the electrodes, even if the nanocrystals do not stick; however, this is not very important because it would mean more charges are collected than nanocrystals (and this is not seen) and (given the mobility measurements) the charge state of the nanocrystals would need to change rapidly in solution (and such a change appears to be slow on these time scales).

After the addition of excess TOPO, the nanocrystals might transfer charge but not stick because of the favorable solvation energy in hexane originating from the large number of ligands present on the surface. It is also possible that a full ligand shell of TOPO/TOPSe acts as an insulating layer, thus preventing the transfer of charge to the film surface.

Deposition may stop after the negative nanocrystals are depleted, because negative counterions do not transfer charge at the positive electrode to counter the transfer of charge from the remaining positive nanocrystals at the negative electrode. Therefore, during deposition most of the current is due to charge transfer from the nanocrystals and not the counterions. The baseline level at the end of the deposition process is higher than the current due to pure TOPO, which indicates that additional ionic impurities may be present in solution after the growth process, and these impurities may contribute to the measured current.

Figure 2a suggests that negative nanocrystals re-form after a deposition during which all of the negative nanocrystals have been extracted. This is confirmed by the use of the solution to deposit new films on both electrodes and the increase in current relative to that at the end of the initial run. This is consistent with the further dissociation or migration of ligands on the nanocrystal surface with time and the exposing of new surface sites, but this is not fast enough for deposition to continue in the initial run.

The ratio of the number of 3.2 nm nanocrystals deposited to the number of charges collected was $\sim 2-3$ using the second and third calibration methods and $\sim 10$ using the first one. Even though the empirical extinction coefficients of the first exciton peak reported by Yu et al.[17] used in the first method are relatively insensitive to surface preparation and ligand type, it is surprising that it leads to a result that is very different than the other two methods. In a previous study,[11] the ratio was determined to be even higher, $\sim 21$ for a 45 min long deposition, by using transmission spectroscopy and the mass of the nanocrystals (which may have been measured after the incomplete removal of solvent) to determine the number of deposited nanocrystals, and it is expected to be less accurate. The number of nanocrystals deposited per charge collected may be somewhat larger than one. If so, this could suggest (1) aggregates of a few nanocrystals may be deposited (some of which are neutral) (but under conditions of smooth EPD film formation light scattering of the solution does not indicate significant aggregation), (2) (singly) charged nanocrystals could drag other nanocrystals along with them onto the electrodes, (3) some nanocrystals are attracted to the electrodes and stick there but transfer charge to another nanocrystal in solution and not to the electrode, or (4) some of the counterions surrounding the charged nanocrystal transfer charge (however this is dubious for singly charged nanocrystals and the cessation of EPD with negative nanocrystal depletion suggests that "isolated" counterions do not transfer charge to the electrode).

*4.2.3. Sticking to the Surface.* Under conditions of EPD of high-quality films, most nanocrystals stick to the surface after charge transfer, because otherwise many neutral nanocrystals would likely have been seen in the mobility measurements after deposition. It is possible that the charge-transfer process increases the sticking probability (in hexane).

Films form in hexane and hexane/octane, but not in chloroform, likely because the TOPO ligands are very soluble in chloroform. After cross-linking with 1,7-heptanediamine, the films do not dissolve in chloroform.[12]

Although the addition of TOPO to the nanocrystal solution appears to make the charge distribution more negative, in most cases there appear to still be both positive and negative nanocrystals, and so the change in the nanocrystal charges does not explain why EPD does not occur from solutions with added TOPO. It is likely due to the prevention of charge transfer at the surface by the added ligands on the core and/or the decreased stickiness of the nanocrystals after charge transfer because of the ligands added to the core (or the related phenomenon due to the added ligands in solution). In this latter mechanism the solvation energy of the nanocrystal exceeds the interparticle van der Waals attractive energy. This mechanism would also account for the dissolution of EPD films when TOPO is added in situ before drying.

## 5. Conclusions

For nanocrystals to be electrophoretically deposited, they need to be charged and be able to transfer charge to and then stick to the electrodes. $\zeta$ potential (electrophoretic mobility), photoluminescence, and other measurements suggest that the removal of the phosphine and phosphine oxide surface ligands from the CdSe nanocrystal cores strongly influences the surface charge of the nanocrystals, indicating that nanocrystals may be charged due to unpassivated surface sites. The removal of surface ligands also makes them more "sticky" by reducing the solubilization energy in the solvent and may help with charge transfer at the electrode surfaces. This explains why the nanocrystals need to be washed to enable the formation of smooth films.

$\zeta$ potential measurements suggest that the concentrations of positively and negatively charged nanocrystals in solution are not equal, so there are clearly counterions present in solution. However, the formation of films of equal thickness on both electrodes suggests that the current observed during the deposition process arises mostly from the charged nanocrystals. The films can be grown only up to a certain maximum thickness because the limiting factor is the depletion of the negatively or positively charged nanocrystals, whichever has the lower concentration (which are the negatively charge nanocrystals here). This model seems to be broadly generalizable to CdSe nanocrystals of different sizes and to mixtures of CdSe nanocrystals and will also likely be applicable to other colloidal nanocrystals.

Ligands play a very significant role in influencing the physical properties of colloidal nanocrystals. Adjusting the ligand

chemistry will help to obtain control over the charging of nanocrystals and will enable the optimization of the electrophoretic deposition process.

**Acknowledgment.** This work was supported primarily by the MRSEC program of the National Science Foundation under Award No. DMR-0213574 and by the New York State Office of Science, Technology, and Academic Research (NYSTAR). Partial support of this project from the NSEC program of the National Science Foundation under Award No. CHE-0641523 is also acknowledged. We thank B. Bilyeu and M. Steigerwald for valuable discussions regarding TGA analysis.

**Supporting Information Available:** Further data concerning the ICP−AES, TGA, ζ potential, and mobility distributions and light scattering data and analysis. This material is available free of charge via the Internet at http://pubs.acs.org.

## References and Notes

(1) Russel, B. W.; Saville, A. D.; Schowalter, R. W. *Colloidal Dispersions*; Cambridge University Press: New York, 1988.
(2) Morrison, I. D. *Colloids Surf., A* **1993**, *71*, 1−37.
(3) Chen, I. *Langmuir* **1996**, *12*, 3437−3441.
(4) Chen, I.; Mort, J.; Machonkin, M. A. *Langmuir* **1997**, *13*, 5036−5040.
(5) Kosmulski, M. *Colloids Surf., A* **1999**, *159*, 277−281.
(6) Hsu, M. F.; Dufresne, E. R.; Weitz, D. A. *Langmuir* **2005**, *21*, 4881−4887.
(7) Shevchenko, E. V.; Talapin, D. V.; O'Brien, S.; Murray, C. B. *J. Am. Chem. Soc.* **2006**, *128* (11), 3620−3637.
(8) Shevchenko, E. V.; Talapin, D. V.; Kotov, N. A.; O'Brien, S.; Murray, C. B. *Nature* **2006**, *439*, 55−59.
(9) Si, S.; Mandal, T. K. *Langmuir* **2007**, *23* (1), 190−195.
(10) Pons, T.; Uyeda, H. T.; Medintz, L. I.; Mattoussi, H. *J. Phys. Chem. B* **2006**, *110*, 20308−20316.
(11) Islam, M. A.; Herman, I. P. *Appl. Phys. Lett.* **2002**, *80* (20), 3823−3825.
(12) Islam, M. A.; Xia, Y.; Telesca, D. A.; Steigerwald, M. L.; Herman, I. P. *Chem. Mater.* **2004**, *16* (1), 49−54.
(13) Murray, C. B.; Norris, D. J.; Bawendi, M. G. *J. Am. Chem. Soc.* **1993**, *115*, 8706−8715.
(14) Islam, M. A.; Xia, Y.; Steigerwald, M. L.; Yin, M.; Liu, Z.; O'Brien, S. *Nano Lett.* **2003**, *3* (11), 1603−1606.
(15) Islam, A. M. Ph. D. Thesis, Columbia University, 2003.
(16) Skoog, D. A.; Holler, F. J.; Nieman, T. A. *Principles of Instrumental Analysis*, 5th ed.; Brooks Cole: Pacific Grove, CA, 1997.
(17) Yu, W. W.; Qu, L.; Guo, W.; Peng, X. *Chem. Mater.* **2003**, *15*, 2854−2860.
(18) Kuno, M.; Lee, J. K.; Dabbousi, B. O.; Mikulec, F. V.; Bawendi, M. G. *J. Chem. Phys.* **1997**, *106* (26), 9869−9882.
(19) Hunter, J. R. *Foundations of Colloid Science*; Oxford University Press: New York, 2001.
(20) Scott, G. D. *Nature* **1960**, *188*, 908−909.
(21) Scott, G. D.; Kilgour, D. M. *Br. J. Appl. Phys.* **1969**, *2*, 863−866.
(22) Onoda, G. Y.; Liniger, E. G. *Phys. Rev. Lett.* **1990**, *64* (22), 2727−2730.
(23) Majetich, S.; Newbury, J.; Newbury, D. *Mater. Res. Soc. Symp. Proc.* **1994**, *332*, 321−326.
(24) Kalyuzhny, G.; Murray, R. W. *J. Phys. Chem. B* **2005**, *109*, 7012−7021.
(25) Tomfohr, J. K.; Sankey, O. F. *Phys. Rev. B* **2002**, *65*, 245105(1−12).
(26) Alivisatos, A. P. *J. Phys. Chem.* **1992**, *100*, 13226−13239.
(27) Krishnan, R.; Hahn, M. A.; Yu, Z.; Silcox, J.; Fauchet, P. M.; Krauss, T. D. *Phys. Rev. Lett.* **2004**, *92* (21), 216803(1)−216803(4).
(28) *Handbook of Chemistry and Physics*, 67th ed.; CRC Press: Boca Raton, FL, 1986.
(29) Jia, S.; Banerjee, S.; Herman, I. P. Unpublished results.
(30) Kagan, C. R.; Murray, C. B.; Nirmal, M.; Bawendi, M. G. *Phys. Rev. Lett.* **1996**, *76* (9), 1517−1520.